

Renormalization group analysis of noisy neural field

Jie Zang (臧杰),^{1,2} Pascal Helson,³ Shenquan Liu (刘深泉),¹ Arvind Kumar,^{3,*} and Dhrubaditya Mitra^{4,†}

¹*School of Mathematics, South China University of Technology, Guangdong, China.*

²*Division of Computational Science and Technology,
School of Electrical Engineering and Computer Science,
KTH Royal Institute of Technology, Stockholm, Sweden*

³*Division of Computational Science and Technology,
School of Electrical Engineering and Computer Science, KTH Royal Institute of Technology,
Stockholm, Sweden. Science for Life Laboratory, Sweden.*

⁴*Nordita, KTH Royal Institute of Technology and Stockholm University,
Hannes Alfvéns väg 12, 10691 Stockholm, Sweden*

(Dated: March 28, 2025)

Neurons in the brain show great diversity in their individual properties and their connections to other neurons. To develop an understanding of how neuronal diversity contributes to brain dynamics and function at large scales we borrow from the framework of replica methods, that has been successfully applied to a large class of problems with quenched noise in equilibrium statistical mechanics. We analyze two linearized versions of Wilson-Cowan model with random coefficients which are correlated in space. In particular: (A) a model where the properties of the neurons themselves are heterogeneous and (B) where their connectivities are anisotropic. In both of these models, the averaging over the quenched randomness gives rise to additional nonlinearities. These nonlinearities are analyzed within the framework of Wilsonian renormalization group. We find that for Model A, if the spatial correlation of noise decays with distance with an exponent smaller than -2 , at large spatial scales the effect of the noise vanishes. By contrast, for model B, the effect of noise in neuronal connectivity vanishes only if the spatial correlations decay with an exponent smaller than -1 . Our calculations also suggest that the presence of noise, under certain conditions, can give rise to travelling wave like behavior at large scales, although it remains to be seen whether this result remains valid at higher orders in perturbation theory.

I. INTRODUCTION

Neurons in the brain show great diversity in their shapes [1], biophysical properties [2] and spiking patterns [3, 4]. This diversity not only can be observed across brain regions but also within a small network of neurons within a brain region [5–7]. Even neurons within a single “cell type” does not have the same structure and response [6, 8, 9]. How neuronal diversity contributes to brain dynamics and function is an important question in modern neuroscience. Usually this question is studied using highly simplified models of cortical connectivity such as random networks [10–13] with fixed distance-independent connectivity or locally connected random networks [14–16]. Interesting suggestions have been made on how neuron diversity renders the brain networks robust [17, 18], improves stimulus encoding [4] and contributes to computational repertoire of the network [19, 20]. But the effect of neuron properties on network activity/function is contingent on the network activity regime [21].

However, neurons in the brain are not wired randomly and their connectivity is constrained by both their physical shapes [22] and chemical signatures [23]. To a reasonable approximation, we can assume that connectivity

decreases with distance in a monotonic fashion [24]. Dynamics of such spatial networks with homogeneous neuron properties and connectivity have been extensively studied [14, 16, 25–28]. In spatial networks, neuron diversity is introduced by choosing neuron properties from a distribution [29] and typically spatial correlations in neuron diversity are set to zero. In terms of connectivity, in spatial network models all neurons are assumed to have the same connectivity kernel and connection diversity arises simply due to finite size effects. In these networks, spatial correlation arise in the neuronal connectivity as the connectivity kernel of neighboring neurons overlaps, therefore, similarity in the connectivity also decays monotonically [30]. However, unlike in random networks, in spatial networks it is important to consider how heterogeneity in both connectivity and neuron properties are spatially correlated. Spreizer et al. [15] showed that when neural connectivity is asymmetric (i.e. neurons make some connections preferentially in a certain direction) and the preferred connection of neighboring neurons are similar, travelling waves and spatio-temporal sequence can arise depending on how the spatial correlation decays as a function of distance. Similar effects are likely when spatial correlations are introduced in neuron properties. Besides these insights, dynamical consequences of the spatial distribution of neuron and connectivity diversity are poorly understood.

Here we introduce a theoretical framework to better understand and identify under which conditions spatial correlations in properties of neurons and their connectiv-

* arv Kumar@kth.se

† dhruba.mitra@gmail.com

ity may affect network dynamics and give rise to non-trivial activity patterns.

We assume that the properties and connectivity of the neurons change at a much slower time scales than the network activity dynamics. Therefore, we can consider heterogeneity in neuronal properties and connectivity as quenched noise. We use the framework of classical stochastic fields [31, 32] to develop a theory of fluctuating activity in excitatory-inhibitory (EI) networks. Recently, Tiberi *et al.* [28] have applied the renormalization group (RG) techniques to a prototypical neural field model, specifically a simplified version of the Wilson-Cowan model [25, 33, 34]. The Wilson-Cowan model is a nonlinear integro-differential equation with constant coefficients driven by a stochastic noise. Under certain simplifying assumptions Tiberi *et al.* [28] reduced this to a nonlinear partial differential equation (PDE) with constant coefficients driven by a stochastic noise. We introduce quenched randomness into this model by changing certain coefficients in the PDE to random functions of space. This makes the model inhomogeneous and anisotropic at small scales, but *statistically* homogeneous and isotropic at large scales. We then average over the quenched noise using the replica trick and extract an effective theory at large scales.

Our theory suggests that when spatial correlations in neuron heterogeneity decays with distance with an exponent smaller than -2 , at large spatial scales the effect of this neuron heterogeneity vanishes. By contrast, the effect of neuron connectivity heterogeneity vanishes only when spatial correlations decays with an exponent smaller than -1 . However, if the connectivity correlation decays with an exponent equal to -1 then its effect depends on the network dimensions. Using our theory we derive conditions when heterogeneity in the connectivity may lead to the emergence of non-trivial dynamics e.g. traveling waves. Thus, our work shows the effect of neuron and connectivity diversity goes beyond adding robustness and may generate novel dynamical states depending on the structure of the spatial distribution of these heterogeneity.

II. MODEL

We start with a neural field following the stochastic Wilson-Cowan equation:

$$\tau \frac{d\phi}{dt} = -l(\phi) + w * f(\phi) + \sqrt{\tau}I, \quad (1)$$

where $\phi(\mathbf{x}, t)$ represents the neural activity evolving in time t over the spatial domain $\mathbf{x} \in \mathbb{R}^d$. Here, τ is the characteristic timescale, $w(\mathbf{x} - \mathbf{y})$ is the connectivity kernel which weights the input from the neural state at position \mathbf{x} to that at position \mathbf{y} through spatial convolution denoted by $*$, and I is a Gaussian noise with zero mean and correlation

$$\langle I(\mathbf{x}, t)I(\mathbf{y}, s) \rangle = D\delta^d(\mathbf{x} - \mathbf{y})\delta(t - s). \quad (2)$$

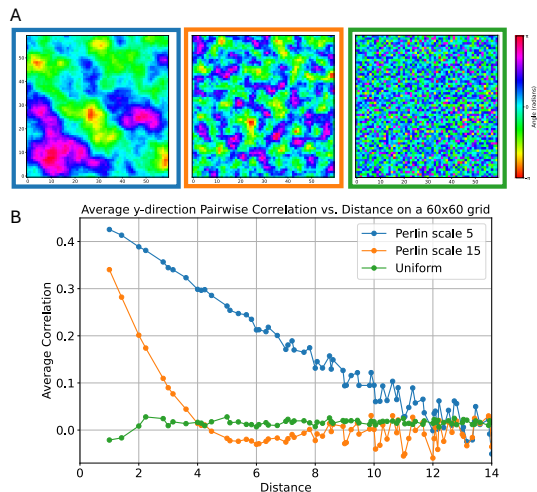


FIG. 1. **A** Three examples of Perlin noise maps (scales 5, 15 and uniform) illustrating the possible connectivity map a neural network can have. Here the values are the angles representing the preferred outgoing direction of each neuron placed on a regular 60 by 60 grid. **B** The corresponding correlation between directions in the y direction ($\sin(\text{angle})$) with respect to the distance between neurons.

Starting from Wilson-Cowan model, Tiberi *et al.* [28] derived a neural field under the assumptions of homogeneity and isotropy:

$$\partial_t \phi = \sum_{n=1}^{\infty} [-A_n + B_n \nabla^2] \phi^n + I. \quad (3)$$

Here A_n , B_n are constants and ∇^2 is the Laplacian operator accounting for spatial diffusion. This model is derived from the Wilson-Cowan equation by expanding the functions $l(\phi)$ and $f(\phi)$ in a Taylor series in ϕ and by expanding the kernel and then ignoring spatial derivatives of fourth order and higher and setting the characteristic time scale $\tau = 1$. In the spirit of constructing Landau-like field theories, (3) is the simplest model we can write for a scalar field (ϕ) under the given symmetries (homogeneity and isotropy) and two additional constraints: the interactions between neurons are local and we ignore derivatives of fourth order and higher.

A. Scaling

Let us first study (3) under the rescaling of space and time. We first select a subset of terms of (3) such that

$$\partial_t \phi = B_1 \nabla^2 \phi + I. \quad (4)$$

This is the well-known Edwards-Wilkinson (EW) equation [35, 36], see also Ref. [37, Chapter 5] for a pedagogic introduction. The EW equation under rescaling $x \rightarrow bx$,

$t \rightarrow b^z t$, $\phi \rightarrow b^\alpha \phi$, and $I \rightarrow b^\lambda I$ gives

$$b^{2\lambda} = b^{-(d+z)} \quad (5a)$$

$$\text{and } \partial_t \phi = b^{z-2} B_1 \nabla^2 \phi + b^{z+\lambda-\alpha} I. \quad (5b)$$

The first equation follows from the scaling of the noise in (2). Demanding that the EW equation remains invariant under rescaling we obtain

$$z = 2, \quad \lambda = -\frac{z+d}{2} \quad \text{and} \quad \alpha = \frac{2-d}{2}, \quad (6)$$

which gives the well-known EW exponents [37, Eq. 5.16]. Next we note how (3) behaves under the same rescaling,

$$\begin{aligned} \partial_t \phi &= (-b^z A_1 + B_1 \nabla^2) \phi + I \\ &+ \sum_{n=2}^{\infty} \left[-b^{(n-1)\alpha+z} A_n + b^{(n-1)\alpha+z-2} B_n \nabla^2 \right] \phi^n. \end{aligned} \quad (7)$$

Substituting the values of α and z from (6) we find that in the limit $b \rightarrow \infty$ (coarse graining):

- The terms $-A_n \phi^n$ scale as $b^{(n-1)(2-d)/2+2}$. If the exponent $(n-1)(2-d)/2+2 < 0$ then all these terms go to zero. This happens for $d > 2+4/(n-1)$. At $d = 2$ all these terms diverge as b^2 .
- The terms $-B_n \phi^n$ for $n \geq 2$ scale as $b^{(n-1)(2-d)/2}$. If the exponent $(n-1)(2-d)/2 < 0$ then all these terms go to zero. This happens for $d > 2$.

Thus we conclude that at $d = 2$ (3) must have the following form under coarse-graining

$$\partial_t \phi = \sum_{n=1}^{\infty} [-b^2 A_n + B_n \nabla^2] \phi^n + I. \quad (8)$$

We are left with two choices. One, we must have the infinity of terms $A_n \phi^n$ and $B_n \nabla^2 \phi^n$ present in the model. The simple scaling of EW model does not hold any longer. Two, we must ignore – by hand set $A_n = 0$ – and still have the infinity of terms $B_n \nabla^2 \phi^n$. In this case too, the simple EW scaling does not hold because there is no *a-priori* reason why the terms nonlinear in ϕ should obey the simple scaling obtained from the linear EW equation. Tiberi *et al.* [28] have taken the second choice and then arbitrarily limited B_n up to $n = 2$. They stated that due to the balance between excitatory and inhibitory inputs in brain networks the terms $A_n \phi^n$ must be zero. Fundamentally speaking, this is a mistaken conclusion. Even a very small A_n for all dimensions $d \geq 2$ will coarse-grain to very large values. In what follows, we consider the possibility that the cancellation is not exact.

B. Models with quenched noise

The Wilson-Cowan model applies at a scale that contains many neurons – it is already a model at mesoscopic

scale. Neurons themselves have significant inhomogeneity – even neurons of same cell type show significant variation between one another. The coefficients A_n are supposed to model *on-site* property of a group of neurons hence they are likely to vary in space in a random manner. As this emerges after averaging over a group of neurons we expect this variation to be less than the variation between properties of individual neurons. As the properties of the neurons do not change over the time scales we consider [38] this noise to be quenched. We assume that this noise is self-averaging and following Ref. [28] we assume its mean to be zero. In particular, we consider A_1 to be a Gaussian random function of space with zero mean and all other $A_n = 0$. We want to focus on the possible effect this randomness may have. To be able to do this in the simplest case, we also set $B_n = 0$ for all $n \geq 2$. Then our model becomes

$$\partial_t \phi = (-g_0 \mathbf{m} + g_2 \nabla^2) \phi + I. \quad (9a)$$

$$\text{where } \langle \mathbf{m}(\mathbf{x}) \mathbf{m}(\mathbf{y}) \rangle = M(\mathbf{r}). \quad (9b)$$

Here, for convenience we have renamed A_1 to \mathbf{m} (and multiplied it with a coupling parameter g_0) and B_1 to g_2 . We assume that the correlation function falls off in space like a power-law: $M(\mathbf{r}) \sim r^{-\gamma}$. This model is isotropic and *statistically* homogeneous. In the rest of this paper we shall call this **Model A**.

Note next that the connection between groups of neurons is also not a constant. In particular, a group of neurons can have stronger connections to another group in a particular direction than other directions. The connections between groups of neurons are not necessarily isotropic. Again, we assume that the anisotropy averages to zero at large scales – it is a small scale quenched noise. This allows us to introduce a new noisy term to the model of Ref. [28], in particular, we consider the model:

$$\partial_t \phi = (-g_1 \mathbf{m} \cdot \nabla + g_2 \nabla^2) \phi + I, \quad (10a)$$

$$\text{where } \langle m_i(\mathbf{x}) m_j(\mathbf{y}) \rangle \equiv M_{ij}(\mathbf{r}) = \delta_{ij} M(\mathbf{r}) \quad (10b)$$

with $M(\mathbf{r}) \sim r^{-\gamma}$ and m_i is the i^{th} component of the vector \mathbf{m} . The local anisotropy is characterized by a vector noise \mathbf{m} which is Gaussian, zero mean, and covariance M given in (10). Here and henceforth we use the notation that repeated indices are summed. We shall call this model **Model B**.

Of course, in reality, both the noises are present together and there may even be some correlation between them. To keep our analysis as simple as possible we limit ourselves to two separate models with two different kinds of noise. Under rescaling $\mathbf{m} \rightarrow b^{-\gamma} \mathbf{m}$, the term g_0 scales as $g_0 b^{z-\gamma}$ and g_1 scales as $g_1 b^{z-\gamma-1}$. Hence under the EW scaling these terms remain relevant. In what follows, we shall describe the key steps in renormalization group analysis of Model A. For Model B, whose analysis proceeds along a very similar line, we shall skip the steps and write down the flow equations directly.

III. RESULTS

A. Replica action for Model A

To analyze the stochastic PDE of Model A, we use the MSRDJ (Martin-Siggia-Rose-De Dominicis-Janssen) path-integral formalism [39–41]. In addition to the usual formalism, our model contains quenched noise. Let us first consider this model with one realization of the quenched noise. We rewrite our model as

$$\mathcal{L}\phi - \mathbf{I} = 0, \quad (11a)$$

$$\text{where } \mathcal{L} \equiv (\partial_t + g_0 \mathbf{m} - g_2 \nabla^2). \quad (11b)$$

This is a stochastic partial differential equation. The solution consists of finding out the space-time dependent probability distribution function $\mathcal{P}[\phi(\mathbf{x}, \mathbf{t})]$. In the MSRDJ formalism, we write down the corresponding moment generating functional

$$\mathcal{Z}[\phi] = \int \mathcal{D}\Phi \mathcal{D}\phi \delta(\mathcal{L}\phi - \mathbf{I}) \exp\left(-\frac{1}{2} \mathbf{I} \bullet \tilde{\mathbf{D}}^{-1} \bullet \mathbf{I}\right). \quad (12)$$

where $\tilde{\mathbf{D}}$ noise correlation on the right hand side of (2). Here the generating functional is written for one realization of the quenched noise \mathbf{m} . The symbol \bullet is defined in the following way. For two functions $f(\mathbf{x}, \mathbf{t})$ and $g(\mathbf{x}, \mathbf{t})$ and an operator \mathcal{M} ,

$$f \bullet \mathcal{M} \bullet g \equiv \int d^d x d^d y dt ds f(\mathbf{x}, \mathbf{t}) \mathcal{M}(\mathbf{x}, \mathbf{t}, \mathbf{y}, s) g(\mathbf{y}, s) \quad (13a)$$

$$\text{and } f \bullet g \equiv \int d^d x dt f(\mathbf{x}, \mathbf{t}) g(\mathbf{x}, \mathbf{t}). \quad (13b)$$

Now we introduce an additional auxiliary field Φ to rewrite the functional δ function in (12) as

$$\mathcal{Z}[\phi] = \int \mathcal{D}\Phi \mathcal{D}\phi \mathcal{D}\mathbf{I} \exp\left[i\Phi \bullet (\mathcal{L}\phi - \mathbf{I}) - \frac{1}{2} \mathbf{I} \bullet \tilde{\mathbf{D}}^{-1} \bullet \mathbf{I}\right]. \quad (14)$$

Integrating over the Gaussian noise \mathbf{I} , we obtain

$$\mathcal{Z}(\mathbf{J}, \mathbf{B}) = \int \mathcal{D}\Phi \mathcal{D}\phi \exp\left[i\Phi \bullet \mathcal{L}\phi - \frac{1}{2} \Phi \bullet \tilde{\mathbf{D}} \bullet \Phi + \mathbf{J} \bullet \phi + \mathbf{B} \bullet \Phi\right]. \quad (15)$$

Here, in addition, we have introduced two source functions $\mathbf{J}(\mathbf{x}, \mathbf{t})$ and $\mathbf{B}(\mathbf{x}, \mathbf{t})$ such that taking functional derivatives with respect to them we can calculate any moment of ϕ and Φ . The path-integral is bilinear in ϕ and Φ , i.e., it can be evaluated exactly and all moments, e.g., $\langle \Phi \phi \rangle$ and $\langle \phi \phi \rangle$ can be calculated exactly. Then these moments must be averaged over the statistics of the quenched noise \mathbf{m} . If we are to calculate all the moments, then it is best to calculate $\langle \ln \mathcal{Z}(\mathbf{J}, \mathbf{B}) \rangle_{\mathbf{m}}$ where $\langle \cdot \rangle_{\mathbf{m}}$ denotes averaging over the statistics of \mathbf{m} . The standard technique is to use the replica trick [42, 43], which starts by recognizing that

$$\ln \mathcal{Z} = \lim_{N \rightarrow 0} \frac{\mathcal{Z}^N - 1}{N}. \quad (16)$$

The trick consists of first calculating $\langle \mathcal{Z}^N \rangle_{\mathbf{m}}$, for any integer N and then taking the limit $N \rightarrow 0$. The product of N path-integrals is

$$\mathcal{Z}^N = \int \prod_{\alpha}^N \mathcal{D}\Phi_{\alpha} \mathcal{D}\phi_{\alpha} \exp\left[\sum_{\alpha}^N (S_{\alpha}^0 + i g_0 \Phi_{\alpha} \bullet \mathbf{m} \bullet \phi_{\alpha})\right]. \quad (17a)$$

$$\text{where } S_{\alpha}^0 \equiv i \Phi_{\alpha} \bullet \mathbf{L} \bullet \phi_{\alpha} - \frac{1}{2} \Phi_{\alpha} \bullet \tilde{\mathbf{D}} \bullet \Phi_{\alpha} \quad (17b)$$

$$\text{and } \mathbf{L} \equiv \partial_t - g_2 \nabla^2. \quad (17c)$$

Next we average this product over the statistics of \mathbf{m} :

$$\langle \mathcal{Z}^N \rangle_{\mathbf{m}} = \int \prod_{\alpha}^N \mathcal{D}\Phi_{\alpha} \mathcal{D}\phi_{\alpha} \exp\left[\sum_{\alpha}^N S_{\alpha}\right] \int \mathcal{D}\mathbf{m} \exp\left[-\frac{1}{2} \mathbf{m} \bullet \mathbf{M}^{-1} \bullet \mathbf{m} + \sum_{\alpha}^N i g_0 \Phi_{\alpha} \bullet \mathbf{m} \bullet \phi_{\alpha}\right] \quad (18a)$$

$$= \int \prod_{\alpha}^N \mathcal{D}\Phi_{\alpha} \mathcal{D}\phi_{\alpha} e^{S_{\text{replica}}}, \quad (18b)$$

$$\text{where } S_{\text{replica}} \equiv \sum_{\alpha}^N S_{\alpha}^0 - g_0^2 \frac{1}{2} \sum_{\alpha, \beta}^N \Phi_{\alpha} \bullet \phi_{\alpha} \bullet \mathbf{M} \bullet \Phi_{\beta} \bullet \phi_{\beta}. \quad (18c)$$

Here in the last step we have done the Gaussian integration over the distribution of \mathbf{m} to obtain the replica action, S_{replica} . The result is a bi-quadratic term containing both Φ and ϕ coupling the replicas together. This

introduces new effective nonlinearity in our model due to averaging over the noise. The strength of this nonlinear is proportional to g_0^2 .

B. Renormalization group analysis

Henceforth we follow the standard prescription of Wilsonian momentum shell renormalization group [see, e.g., 44, for a pedagogical introduction]. Details of the calculation are given in Appendix A. The calculations are done in Fourier space:

$$\phi(\mathbf{k}, \omega) \equiv \int \phi(\mathbf{x}, t) e^{i\mathbf{k}\cdot\mathbf{x} - i\omega t} d^d \mathbf{x} dt, \quad (19a)$$

$$\Phi(\mathbf{k}, \omega) \equiv \int \Phi(\mathbf{x}, t) e^{i\mathbf{k}\cdot\mathbf{x} - i\omega t} d^d \mathbf{x} dt. \quad (19b)$$

To avoid proliferation of symbols, we use the same symbol for a field in real and Fourier space. In case of possible confusion, we distinguish them by explicitly giving their argument. In Fourier space our problem has a high \mathbf{k} cutoff (ultraviolet cutoff) Λ . We consider a thin shell in Fourier space between Λ/b to Λ . Later we shall take the limit $b \rightarrow 1$. We separate both ϕ and Φ in two, one with wavevector $|\mathbf{k}|$ less than Λ/b and the other with wavevector lying within the thin shell Λ/b to Λ . They are denoted respectively by $\phi^<$ ($\Phi^<$) and $\phi^>$ ($\Phi^>$), i.e.,

$$\phi = \phi^< + \phi^>, \quad (20a)$$

$$\Phi = \Phi^< + \Phi^>. \quad (20b)$$

The fields with label $>$ are called ‘‘fast’’ modes and with label $<$ are called ‘‘slow’’. As we eventually take the limit $b \rightarrow 1$, we rewrite $b = \exp(\delta\ell) \approx 1 + \delta\ell$. The key idea of Wilsonian RG is to integrate over the fast modes to write an effective theory for the slow mode. The crucial limitation is that the effective theory is constrained to have the same functional form as the original one we started with but with coupling constants – D , g_0 and g_2 – each becoming a function of scale, ℓ . We remind the reader that one of the key properties we are trying to capture is the possible appearance of traveling wave like behavior due to the presence of noise. To be able to capture that within our model we write $g_2 = \beta + i\Omega$. At small scale $\Omega \ll \beta$. The appearance of large scale traveling waves is detected if Ω grows under the RG transformation.

In the limit $N \rightarrow 0$ and at the level of one-loop, the RG flow equations for D , g_0 , β , and Ω for Model A are:

$$\frac{dg_0}{d\ell} = g_0(z - \gamma) \quad (21a)$$

$$\frac{d\beta}{d\ell} = \beta \left(z - 2 - \frac{g_0^2 Q_d}{\beta^2 + \Omega^2} \left(\frac{1}{k^2} + \frac{4}{d} - 1 \right) \right) \quad (21b)$$

$$\frac{d\Omega}{d\ell} = \Omega \left(z - 2 + \frac{g_0^2 Q_d}{\beta^2 + \Omega^2} \left(\frac{1}{k^2} + \frac{4}{d} - 1 \right) \right) \quad (21c)$$

$$\frac{dD}{d\ell} = D \left(z - d - 2\alpha + \frac{g_0^2 Q_d}{\beta^2 + \Omega^2} \right), \quad (21d)$$

where $Q_d \equiv (M(1)S_d)/(2\pi)^{d+1}$. There are several key aspects to notice in these flow equations.

1. There is no correction at this order to g_0 . In RG of the KPZ equation, the correction to the vertex is also zero *to all orders* [37]. This is because the KPZ equation can be mapped to the Burgers equation which has Galilean symmetry which dictates that the vertex does not renormalize. This does not hold in the present case. We expect corrections to g_0 at higher order in perturbation theory.
2. In principle, we must take the limit $k \rightarrow 0$ in these equations. This would make the flow equations diverge, i.e., the theory has divergences at small k – infra-red (IR) divergences. Such divergences often plague RG of non-equilibrium systems. We may be able to control such divergence by resorting to non-perturbative functional renormalization group method [45–48]. This is beyond that scope of the present work.
3. For $z = 2$ and $\gamma < 2$, these equations admit one fixed point which corresponds to $g_0 = 0$. We recover the properties of the noiseless equations. This is our first important result. If the noise correlation decays in space fast enough ($\gamma > 2$) the role of the noise can be safely ignored.
4. For $z = 2$ and $\gamma = 2$, g_0 remains unchanged. The coefficient β decreases and Ω increases as we go to large scales – traveling waves dominate the large scale behavior of the system even for a small g_0 . This is a very interesting possibility but calculation of higher order terms in perturbation theory and a proper control of IR divergence is necessary before we can actually reach this conclusion.
5. For $z = 2$ and $\gamma > 2$, the strength of the nonlinearity (or quenched noise), g_0 , grows without bound as we go to large scales. In this case, calculation of higher order terms in perturbation theory is necessary to make any meaningful predictions.

C. RG flow equations for Model B

Instead of the scalar quenched noise in Model A, model B has vector noise that encodes the local anisotropy. Following the same method as for Model A, see section B, we obtain the following flow equations:

$$\frac{dg_1}{d\ell} = g_1(z - \gamma - 1) \quad (22a)$$

$$\frac{d\beta}{d\ell} = \beta \left(z - 2 + \frac{g_1^2 Q_d}{\beta^2 + \Omega^2} \left(1 - \frac{2}{d} \right) \right) \quad (22b)$$

$$\frac{d\Omega}{d\ell} = \Omega \left(z - 2 - \frac{g_1^2 Q_d}{\beta^2 + \Omega^2} \left(1 - \frac{2}{d} \right) \right) \quad (22c)$$

$$\frac{dD}{d\ell} = D \left(z - d - 2\alpha + \frac{g_1^2 Q_d}{\beta^2 + \Omega^2} \right) \quad (22d)$$

where $Q_d \equiv (M(1)S_d)/(2\pi)^{d+1}$.

There are several key aspects to notice in these flow equations.

1. Similar to Model A there is no correction at this order to g_0 . We expect corrections to g_0 at higher order in perturbation theory.
2. In contrast to Model A there are no IR divergences.
3. For $z = 2$ and $\gamma < 1$, these equations admit one fixed point which corresponds to $g_0 = 0$. We recover the properties of the noiseless equations. This is our second important result. If the noise correlation decays in space fast enough ($\gamma > 1$) the role of the noise can be safely ignored.
4. For $z = 2$ and $\gamma = 1$, g_0 remains unchanged. At this order, the behavior is now qualitatively different for different dimensions. For $d > 2$ the coefficient β increases and Ω decreases as we go to large scales – there are no travelling waves. Although the noise cannot be ignored at large scales. For $d < 2$, similar to Model A, the coefficient β decreases and Ω increases as we go to large scales – traveling waves dominate the large scale behavior of the system even for a small g_0 . Again, this intriguing possibility can be confirmed only after calculation of higher order terms in perturbation theory and a proper control of IR divergence.
5. For $z = 2$ and $\gamma > 1$, the strength of the nonlinearity (or quenched noise), g_0 , grows without bound as we go to large scales. In this case, calculation of higher order terms in perturbation theory is necessary to make any meaningful predictions.

IV. SUMMARY

Our goal in this paper is to introduce the framework of replica renormalization group to problems in neuroscience. The replica method has been successfully applied to a large class of problems with quenched noise in equilibrium statistical mechanics [43]. Given the natural heterogeneity of neural networks in brain it seems to be well suited to extract large scale behavior in neuroscience too. We apply it to two models, one where the properties of neurons themselves are heterogeneous and the other where the connectivity of the neurons is anisotropic. Our calculations show that, for the former, if the spatial correlation of noise decays with distance with an exponent smaller than -2 , at large spatial scales the effect of this neuron heterogeneity vanishes. By contrast, the effect of heterogeneity in neuronal connectivity vanishes only when spatial correlations decays with an exponent smaller than -1 . Our calculations also suggests that the presence of noise can give rise to travelling wave like behavior at large scale, although it remains to be seen whether this result remains valid at higher orders in perturbation theory.

ACKNOWLEDGMENTS

We thank Hauke Wernecke for providing the code to simulate Perlin noise (Fig. 1). This work was funded in parts by StratNeuro (to AK), Digital Futures grants (to AK and PH), the Inst. of Advanced Studies, University of Strasbourg, France Fellowship (to AK), and the National Natural Science Foundation of China under Grant No. 11572127 and 11872183 (to SL). DM acknowledges the support of the Swedish Research Council Grant No. 638-2013-9243. DM thanks Rahul Pandit for useful discussions.

-
- [1] H. Peng, P. Xie, L. Liu, X. Kuang, Y. Wang, L. Qu, H. Gong, S. Jiang, A. Li, Z. Ruan, *et al.*, Morphological diversity of single neurons in molecularly defined cell types, *Nature* **598**, 174 (2021).
 - [2] L. Lim, D. Mi, A. Llorca, and O. Marín, Development and functional diversification of cortical interneurons, *Neuron* **100**, 294 (2018).
 - [3] P. Le Merre, K. Heining, M. Slashcheva, F. Jung, E. Moysiadou, N. Guyon, R. Yahya, H. Park, F. Wernstl, and M. Carlén, A prefrontal cortex map based on single neuron activity, *bioRxiv*, 2024 (2024).
 - [4] M. N. Insanally, B. F. Albanna, J. Toth, B. DePasquale, S. S. Fadaei, T. Gupta, O. Lombardi, K. Kuchibhotla, K. Rajan, and R. C. Froemke, Contributions of cortical neuron firing patterns, synaptic connectivity, and plasticity to task performance, *Nature communications* **15**, 6023 (2024).
 - [5] G. Stanley, O. Gokce, R. C. Malenka, T. C. Südhof, and S. R. Quake, Continuous and discrete neuron types of the adult murine striatum, *Neuron* **105**, 688 (2020).
 - [6] M. S. Cembrowski and V. Menon, Continuous variation within cell types of the nervous system, *Trends in Neurosciences* **41**, 337 (2018).
 - [7] J. B. Isbister, A. Ecker, C. Pokorny, S. Bolaños-Puchet, D. E. Santander, A. Arnaudon, O. Awile, N. Barros-Zulaica, J. B. Alonso, E. Boci, *et al.*, Modeling and simulation of neocortical micro-and mesocircuitry. part ii: Physiology and experimentation, *bioRxiv*, 2023 (2023).
 - [8] K. Angelo, E. A. Rancz, D. Pimentel, C. Hundahl, J. Hannibal, A. Fleischmann, B. Pichler, and T. W. Margrie, A biophysical signature of network affiliation and sensory processing in mitral cells, *Nature* **488**, 375 (2012).
 - [9] F. Scala, D. Kobak, M. Bernabucci, Y. Bernaerts, C. R. Cadwell, J. R. Castro, L. Hartmanis, X. Jiang, S. Laturus, E. Miranda, *et al.*, Phenotypic variation of transcriptional cell types in mouse motor cortex, *Nature* **598**, 144 (2021).
 - [10] C. Van Vreeswijk and H. Sompolinsky, Chaos in neuronal networks with balanced excitatory and inhibitory activ-

- ity, *Science* **274**, 1724 (1996).
- [11] N. Brunel, Dynamics of sparsely connected networks of excitatory and inhibitory spiking neurons, *Journal of computational neuroscience* **8**, 183 (2000).
- [12] A. Kumar, S. Schrader, A. Aertsen, and S. Rotter, The high-conductance state of cortical networks, *Neural computation* **20**, 1 (2008).
- [13] S. El Boustani and A. Destexhe, A master equation formalism for macroscopic modeling of asynchronous irregular activity states, *Neural computation* **21**, 46 (2009).
- [14] B. Ermentrout, Neural networks as spatio-temporal pattern-forming systems, *Reports on progress in physics* **61**, 353 (1998).
- [15] S. Spreizer, A. Aertsen, and A. Kumar, From space to time: Spatial inhomogeneities lead to the emergence of spatiotemporal sequences in spiking neuronal networks, *PLoS computational biology* **15**, e1007432 (2019).
- [16] R. Rosenbaum, M. A. Smith, A. Kohn, J. E. Rubin, and B. Doiron, The spatial structure of correlated neuronal variability, *Nature neuroscience* **20**, 107 (2017).
- [17] S. Rich, H. Moradi Chameh, J. Lefebvre, and T. Valiante, Loss of neuronal heterogeneity in epileptogenic human tissue impairs network resilience to sudden changes in synchrony. *cell rep.* **39**, 110863 (2022).
- [18] A. Hutt, S. Rich, T. A. Valiante, and J. Lefebvre, Intrinsic neural diversity quenches the dynamic volatility of neural networks, *Proceedings of the National Academy of Sciences* **120**, e2218841120 (2023).
- [19] G. Marsat and L. Maler, Neural heterogeneity and efficient population codes for communication signals, *Journal of neurophysiology* **104**, 2543 (2010).
- [20] R. Gast, S. A. Solla, and A. Kennedy, Neural heterogeneity controls computations in spiking neural networks, *Proceedings of the National Academy of Sciences* **121**, e2311885121 (2024).
- [21] A. Sahasranamam, I. Vlachos, A. Aertsen, and A. Kumar, Dynamical state of the network determines the efficacy of single neuron properties in shaping the network activity, *Scientific reports* **6**, 26029 (2016).
- [22] X. Jiang, S. Shen, C. R. Cadwell, P. Berens, F. Sinz, A. S. Ecker, S. Patel, and A. S. Tolias, Principles of connectivity among morphologically defined cell types in adult neocortex, *Science* **350**, aac9462 (2015).
- [23] D. L. Barabási and A.-L. Barabási, A genetic model of the connectome, *Neuron* **105**, 435 (2020).
- [24] X. Xu, N. D. Olivas, T. Ikrar, T. Peng, T. C. Holmes, Q. Nie, and Y. Shi, Primary visual cortex shows laminar-specific and balanced circuit organization of excitatory and inhibitory synaptic connectivity, *The Journal of physiology* **594**, 1891 (2016).
- [25] S. Coombes, *Neural fields.*, *Scholarpedia* **1**, 1373 (2006).
- [26] P. C. Bressloff, J. D. Cowan, M. Golubitsky, P. J. Thomas, and M. C. Wiener, Geometric visual hallucinations, euclidean symmetry and the functional architecture of striate cortex, *Philosophical Transactions of the Royal Society of London. Series B: Biological Sciences* **356**, 299 (2001).
- [27] S. Spreizer, M. Angelhuber, J. Bahuguna, A. Aertsen, and A. Kumar, Activity dynamics and signal representation in a striatal network model with distance-dependent connectivity, *Eneuro* **4** (2017).
- [28] L. Tiberi, J. Stapmanns, T. Kühn, T. Luu, D. Dahmen, and M. Helias, Gell-mann-low criticality in neural networks, *Physical review letters* **128**, 168301 (2022).
- [29] A. Kumar, S. Rotter, and A. Aertsen, Conditions for propagating synchronous spiking and asynchronous firing rates in a cortical network model, *Journal of neuroscience* **28**, 5268 (2008).
- [30] C. Mehring, U. Hehl, M. Kubo, M. Diesmann, and A. Aertsen, Activity dynamics and propagation of synchronous spiking in locally connected random networks, *Biological cybernetics* **88**, 395 (2003).
- [31] M. A. Buice and J. D. Cowan, Field-theoretic approach to fluctuation effects in neural networks, *Physical Review E—Statistical, Nonlinear, and Soft Matter Physics* **75**, 051919 (2007).
- [32] M. A. Buice, J. D. Cowan, and C. C. Chow, Systematic fluctuation expansion for neural network activity equations, *Neural computation* **22**, 377 (2010).
- [33] H. R. Wilson and J. D. Cowan, Excitatory and inhibitory interactions in localized populations of model neurons, *Biophysical journal* **12**, 1 (1972).
- [34] H. R. Wilson and J. D. Cowan, A mathematical theory of the functional dynamics of cortical and thalamic nervous tissue, *Kybernetik* **13**, 55 (1973).
- [35] S. Chui and J. Weeks, Dynamics of the roughening transition, *Physical Review Letters* **40**, 733 (1978).
- [36] S. F. Edwards and D. Wilkinson, The surface statistics of a granular aggregate, *Proceedings of the Royal Society of London. A. Mathematical and Physical Sciences* **381**, 17 (1982).
- [37] A.-L. Barabási and H. E. Stanley, *Fractal concepts in surface growth* (Cambridge university press, 1995).
- [38] In practice, neurons are plastic, i.e., their properties change with time but over a time scale that is much slower than the time scales we consider here.
- [39] P. C. Martin, E. D. Siggia, and H. A. Rose, Statistical dynamics of classical systems, *Physical Review A* **8**, 423 (1973).
- [40] H.-K. Janssen, On a lagrangean for classical field dynamics and renormalization group calculations of dynamical critical properties, *Zeitschrift für Physik B Condensed Matter* **23**, 377 (1976).
- [41] C. De Dominicis and L. Peliti, Field-theory renormalization and critical dynamics above t_c : Helium, antiferromagnets, and liquid-gas systems, *Physical Review B* **18**, 353 (1978).
- [42] G. Parisi, The order parameter for spin glasses: a function on the interval 0-1, *Journal of Physics A: Mathematical and General* **13**, 1101 (1980).
- [43] M. Mézard, G. Parisi, and M. A. Virasoro, *Spin glass theory and beyond: An Introduction to the Replica Method and Its Applications*, Vol. 9 (World Scientific Publishing Company, 1987).
- [44] R. Shankar, *Quantum field theory and condensed matter: an introduction* (Cambridge University Press, 2017).
- [45] L. Canet, H. Chaté, B. Delamotte, and N. Wschebor, Nonperturbative renormalization group for the kardar-parisi-zhang equation, *Physical review letters* **104**, 150601 (2010).
- [46] L. Canet, H. Chaté, B. Delamotte, and N. Wschebor, Nonperturbative renormalization group for the kardar-parisi-zhang equation: General framework and first applications, *Physical Review E—Statistical, Nonlinear, and Soft Matter Physics* **84**, 061128 (2011).
- [47] L. Canet, H. Chaté, and B. Delamotte, General framework of the non-perturbative renormalization group for non-equilibrium steady states, *Journal of Physics A:*

Mathematical and Theoretical **44**, 495001 (2011).

- [48] B. Delamotte, An introduction to the nonperturbative renormalization group, in *Renormalization group and effective field theory approaches to many-body systems* (Springer Berlin Heidelberg Berlin, Heidelberg, 2012) pp. 49–132.

Appendix A: Replica Renormalization group analysis for Model A

In this appendix we discuss the RG analysis for Model A. We start with the replica averaged moment generating

$$\langle \mathcal{Z}^N \rangle_m = \int \prod_{\alpha}^N \mathcal{D}\Phi_{\alpha} \mathcal{D}\phi_{\alpha} \exp \left[\sum_{\alpha}^N S_{\alpha} \right] \int \mathcal{D}\mathbf{m} \exp \left[-\frac{1}{2} \mathbf{m} \bullet \mathbf{M}^{-1} \bullet \mathbf{m} + \sum_{\alpha}^N i g_0 \Phi_{\alpha} \bullet \mathbf{m} \bullet \phi_{\alpha} \right] \quad (\text{A1a})$$

$$= \int \prod_{\alpha}^N \mathcal{D}\Phi_{\alpha} \mathcal{D}\phi_{\alpha} e^{S_{\text{replica}}}. \quad (\text{A1b})$$

$$\text{where } S_{\text{replica}} \equiv \sum_{\alpha}^N S_{\alpha}^0 - g_0^2 \frac{1}{2} \sum_{\alpha, \beta}^N \Phi_{\alpha} \bullet \phi_{\alpha} \bullet \mathbf{M} \bullet \Phi_{\beta} \bullet \phi_{\beta}. \quad (\text{A1c})$$

Following the standard prescription of momentum shell renormalization group (RG) [see, e.g., 44, for a pedagogical introduction] calculation we now consider the problem in in Fourier space,

$$\phi(\mathbf{k}, \omega) \equiv \int \phi(\mathbf{x}, t) e^{i\mathbf{k} \cdot \mathbf{x} - i\omega t} d^d \mathbf{x} dt. \quad (\text{A2a})$$

$$\Phi(\mathbf{k}, \omega) \equiv \int \Phi(\mathbf{x}, t) e^{i\mathbf{k} \cdot \mathbf{x} - i\omega t} d^d \mathbf{x} dt. \quad (\text{A2b})$$

To avoid proliferation of symbols, we use the same symbol for a field in real and Fourier space. In case of possible confusion, we distinguish them by explicitly giving their argument. In Fourier space our problem has a high k cutoff (ultraviolet cutoff) Λ . We consider a thin shell in Fourier space between Λ/b to Λ . Later we shall take the limit $b \rightarrow 1$. We separate both ϕ and Φ in two, one

function.

with wavevector $|\mathbf{k}|$ less than Λ/b and the other with wavevector lying within the thin shell Λ/b to Λ . The are denoted respectively by $\phi^{<} (\Phi^{<})$ and $\phi^{>} (\Phi^{>})$, i.e.,

$$\phi = \phi^{<} + \phi^{>}. \quad (\text{A3a})$$

$$\Phi = \Phi^{<} + \Phi^{>}. \quad (\text{A3b})$$

The fields with label $>$ are labeled called ‘‘fast’’ modes and with label $<$ are labeled ‘‘slow’’.

The integration measure in (A1) factorizes into

$$\prod_{\alpha}^N \mathcal{D}\Phi_{\alpha} \mathcal{D}\phi_{\alpha} \rightarrow \prod_{\alpha}^N \mathcal{D}\Phi_{\alpha}^{<} \mathcal{D}\phi_{\alpha}^{<} (\mathcal{D}\Phi_{\alpha}^{>} \mathcal{D}\phi_{\alpha}^{>}). \quad (\text{A4})$$

Let us first consider only the diagonal (and linear) part of the replica action S_{α}^0 . Then the replica action does not couple different replicas. It is sufficient to consider just one replica. The action in Fourier space:

$$S^0(\Phi, \phi) = \int \frac{d^d \mathbf{k}}{(2\pi)^d} \frac{d\omega}{(2\pi)} \left[i\Phi(-\mathbf{k}, -\omega) L \phi(\mathbf{k}, \omega) - \frac{1}{2} \Phi(-\mathbf{k}, -\omega) \tilde{D} \Phi(\mathbf{k}, \omega) \right]. \quad (\text{A5a})$$

$$\text{where } L \equiv g_2 k^2 - i\omega. \quad (\text{A5b})$$

Before we proceed further let us introduce a more compact notation:

1. We shall often suppress the frequency label. More specifically, a term $\delta^d(\mathbf{q})\delta(\omega)$ will be simply written as $\delta(\mathbf{q})$, suppressing the ω label. Similarly a function $\phi(\mathbf{k}, \omega)$ will be simply written as $\phi(\mathbf{k})$. We shall reintroduce the frequency labels explicitly when necessary.

2. We define:

$$\int_{\mathbf{k}}^{>} \equiv \int_{\Lambda/b}^{\Lambda} \frac{d^d \mathbf{k}}{(2\pi)^d} \int_{-\infty}^{\infty} \frac{d\omega}{(2\pi)}. \quad (\text{A6})$$

The action S^0 neatly separates into fast and slow

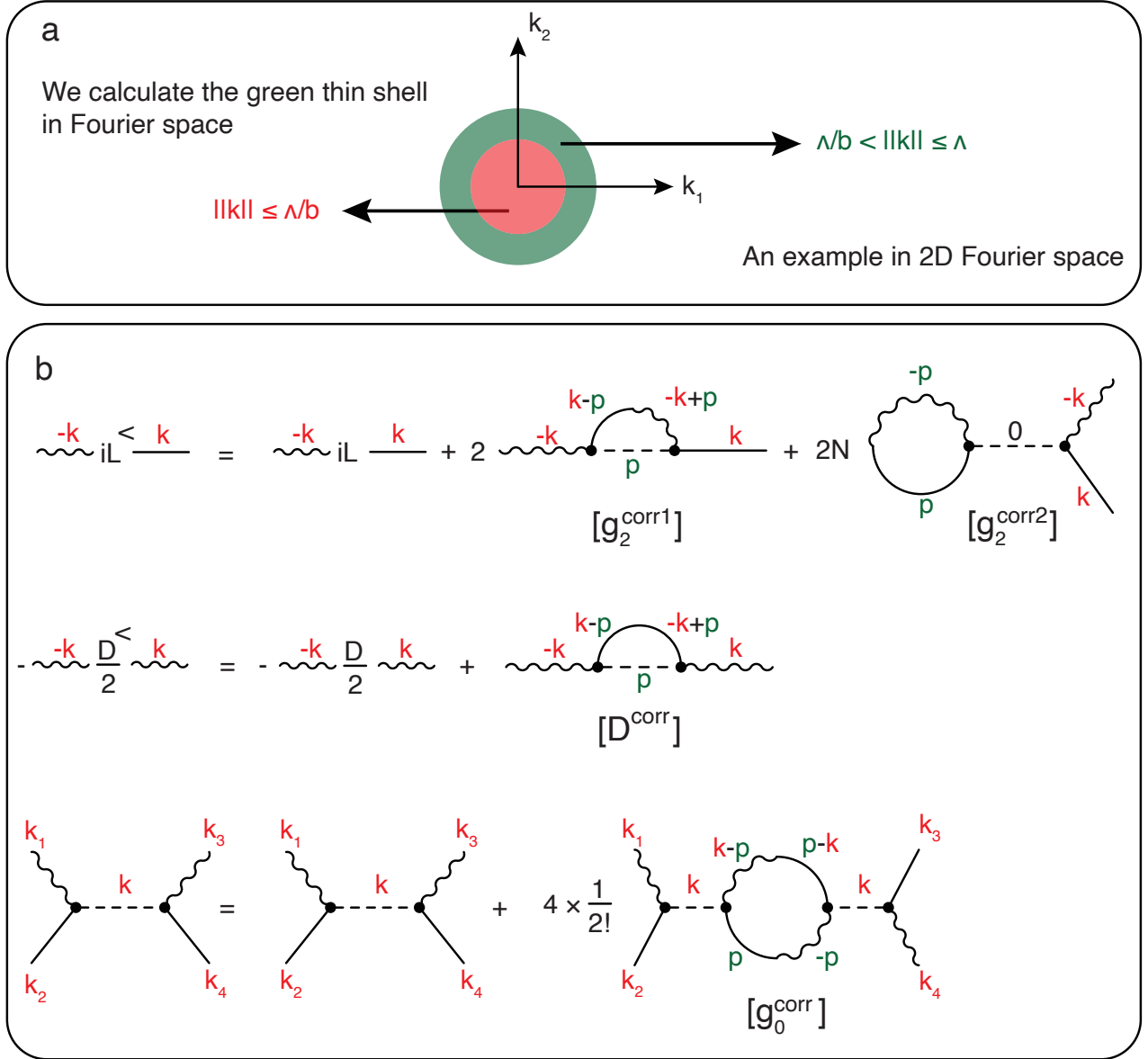


FIG. 2. **a**. An illustration of RG process in 2D dimension. **b**. Feynman diagrams to calculate correction to g_0 , g_2 and D in model A up to one loop order. The short straight lines and short wavy lines denote ϕ and Φ respectively. The long straight line denotes the free correlation function and the long line with one wavy end and other straight end denotes the free Green's function.

modes

The complete replica action:

$$S^0(\Phi, \phi) = S^{0,<}(\Phi^<, \phi^<) + S^{0,>}(\Phi^>, \phi^>) \quad (\text{A7a})$$

$$\text{where } S^{0,<}(\Phi^<, \phi^<) = \int_0^{\wedge/b} \frac{d^d k}{(2\pi)^d} \left[i\Phi^< L\phi^< - \frac{1}{2}\Phi^< \tilde{D}\Phi^< \right] \quad (\text{A7b})$$

$$\text{and } S^{0,>}(\Phi^>, \phi^>) = \int_k^> \left[i\Phi^> L\phi^> - \frac{1}{2}\Phi^< \tilde{D}\Phi^< \right]. \quad (\text{A7c})$$

$$S_{\text{replica}} = \sum_{\alpha}^N S_{\alpha}^{0,<}(\Phi^{<}, \phi^{<}) + \sum_{\alpha}^N S_{\alpha}^{0,>}(\Phi^{>}, \phi^{>}) + S^I(\Phi^{<}, \phi^{<}, \Phi^{>}, \phi^{>}) \quad (\text{A8a})$$

$$\text{where } S^I(\Phi^{<}, \phi^{<}, \Phi^{>}, \phi^{>}) = -g_0^2 \frac{1}{2} \sum_{\alpha, \beta}^N \Phi_{\alpha} \bullet \phi_{\alpha} \bullet M \bullet \Phi_{\beta} \bullet \phi_{\beta}. \quad (\text{A8b})$$

The moment generating function

$$\langle \mathcal{Z}^N \rangle_{\text{m}} = \int \prod_{\alpha}^N \mathcal{D}\Phi_{\alpha}^{<} \mathcal{D}\phi_{\alpha}^{<} e^{S^{0,<}} \int \prod_{\alpha}^N \mathcal{D}\Phi_{\alpha}^{>} \mathcal{D}\phi_{\alpha}^{>} e^{S^{0,>}} e^{S^I} \quad (\text{A9a})$$

$$\equiv \int \prod_{\alpha}^N \mathcal{D}\Phi_{\alpha}^{<} \mathcal{D}\phi_{\alpha}^{<} e^{S^{\text{eff}}(\Phi_{\alpha}^{<}, \phi_{\alpha}^{<})}, \quad (\text{A9b})$$

where the last line defines the effective action S^{eff} . We rewrite the effective action as

$$\begin{aligned} e^{S^{\text{eff}}} &= \frac{\mathcal{Z}_0^{>}}{\mathcal{Z}_0^{<}} \int \prod_{\alpha}^N \mathcal{D}\Phi_{\alpha}^{>} \mathcal{D}\phi_{\alpha}^{>} e^{S^{0,>}} e^{S^I} \quad (\text{A10a}) \\ &= \mathcal{Z}_0^{>} \langle \exp [S^I(\Phi^{<}, \phi^{<}, \Phi^{>}, \phi^{>})] \rangle_0 \quad (\text{A10b}) \end{aligned}$$

$$\text{where } \mathcal{Z}_0^{>} \equiv \int \prod_{\alpha}^N \mathcal{D}\Phi_{\alpha}^{>} \mathcal{D}\phi_{\alpha}^{>} e^{S^{0,>}}. \quad (\text{A10c})$$

Here we define

$$\langle f(\Phi^{>}, \phi^{>}) \rangle_0 \equiv \int \mathcal{D}\Phi_{\alpha}^{>} \mathcal{D}\phi_{\alpha}^{>} e^{S^{0,>}} f(\Phi^{>}, \phi^{>}). \quad (\text{A11})$$

where $f(\Phi^{>}, \phi^{>})$ is any function of $\Phi^{>}$ and $\phi^{>}$. In (A10b) the factor $\mathcal{Z}_0^{>}$ is a number that does not depend on the slow modes, it can be safely ignored. Thus the problem boils down to calculating the effective action by doing the averaging over the Gaussian action of the fast modes in (A10b).

We do this perturbatively through the cumulant expansion

$$\langle e^{g_0^2 \Lambda} \rangle_0 = \exp \left[g_0^2 \langle \Lambda \rangle_0 + g_0^4 \frac{1}{2} \left(\langle \Lambda^2 \rangle_0 - \langle \Lambda \rangle_0^2 \right) + \text{h.o.t.} \right], \quad (\text{A12a})$$

$$\text{where } \Lambda \equiv -\frac{1}{2} \sum_{\alpha, \beta}^N \Phi_{\alpha} \bullet \phi_{\alpha} \bullet M \bullet \Phi_{\beta} \bullet \phi_{\beta}. \quad (\text{A12b})$$

The most convenient way to perform this expansion is to use the Feynman diagrams. The cumulant expansion guarantees that at every order in g_0^2 only the connected diagrams appear.

The integration over the first term in (A12a) is

$$\begin{aligned} g_0^2 \langle \Lambda \rangle_0 &= \int \prod_{\alpha}^N \mathcal{D}\Phi_{\alpha}^{>} \mathcal{D}\phi_{\alpha}^{>} \prod_{\alpha}^N e^{S_{\alpha}^{0,>}} \\ &\quad \left(-\frac{1}{2} g_0^2 \sum_{\alpha, \beta}^N \Phi_{\alpha} \bullet \phi_{\alpha} \bullet M \bullet \Phi_{\beta} \bullet \phi_{\beta} \right). \quad (\text{A13}) \end{aligned}$$

The term in the parenthesis mixes both the fast and the slow and also the replica labels. To proceed further we shall need the ‘‘free’’ Green’s function and the correlation function given by

$$G_0(\mathbf{k}) \equiv \langle \phi_{\alpha}^{>}(\mathbf{k}) \Phi_{\beta}^{>}(-\mathbf{k}) \rangle_0 = -\frac{\delta_{\alpha\beta}}{\omega + i g_2 k^2} \quad (\text{A14a})$$

$$F_0(\mathbf{k}) \equiv \langle \phi_{\alpha}^{>}(\mathbf{k}) \phi_{\beta}^{>}(-\mathbf{k}) \rangle_0 = \frac{D \delta_{\alpha\beta}}{\omega^2 + g_2^2 k^4}, \quad (\text{A14b})$$

$$\text{and } \langle \Phi_{\alpha}^{>}(\mathbf{k}) \Phi_{\beta}^{>}(-\mathbf{k}) \rangle_0 = 0 \quad (\text{A14c})$$

These can be calculated in a straightforward manner from (A1) with the obvious Kronecker delta between replicas.

Returning to (A13), we separate this term into fast and slow modes. We obtain sixteen possible terms of the following types

- Eight terms with odd number of fast modes. They are all zero because the average, $\langle \cdot \rangle_0$ is over a Gaussian weight.
- One term with all the fast modes. This averages to a constant that does not depend on the slow modes. Hence can be ignored.
- One term with all the slow modes. This remains unchanged.
- Six terms with two slow and two fast modes.

Let us now consider the six terms each of which contains two slow and two fast modes. Once we have integrated over the fast modes these terms generate effective coupling between the slow modes. These effective couplings renormalize the coupling constants in the original action. Up to one loop these corrections are given in Fig. 2.

As shown in Fig. 2, the term S_A^I will renormalize g_0 , g_2 , and D and it is given by

$$\begin{aligned} S_A^I &= -g_0^2 \frac{1}{2} \sum_{\alpha, \beta}^N \Phi_\alpha(\mathbf{k}_1) \bullet \Phi_\alpha(\mathbf{k}_2) \bullet M(\mathbf{p}) \bullet \Phi_\beta(\mathbf{k}_3) \bullet \Phi_\beta(\mathbf{k}_4) \\ &\quad \times \delta(\mathbf{k}_1 + \mathbf{k}_2 - \mathbf{p}) \delta(\mathbf{k}_3 + \mathbf{k}_4 + \mathbf{p}) \\ &:= \end{aligned} \quad (A15)$$

Also, without any loss of generality, we set the cutoff $\Lambda = 1$, in other words all the wavevector are henceforth measured in unit of Λ . Thus, we get the correction to D , g_2 and g_0 :

$$D^{\text{corr}} = -\frac{1}{\beta^2 + \Omega^2} \frac{g_0^2 D M(1) S_d}{2(2\pi)^{d+1}} \delta\ell \quad (A16a)$$

$$g_2^{\text{corr1}} = \left(-\frac{\beta - i\Omega}{\beta^2 + \Omega^2} \frac{ig_0^2 M(1) S_d}{2(2\pi)^{d+1}} \right) \delta\ell \left[1 + k^2 \left(\frac{4}{d} - 1 \right) \right] \quad (A16b)$$

$$g_2^{\text{corr2}} = -\frac{ig_0^2 M(0) S_d}{2(2\pi)^d} \delta\ell \quad (A16c)$$

$$g_0^{\text{corr}} = 0 \quad (A16d)$$

Note that the correction to the vertex is zero to this order. In RG of KPZ the correction to vertex is zero to all orders [37]. This is because the KPZ equation can be mapped to the Burgers equation which has Galilean symmetry which dictates that the vertex does not renormalize. In our model, we expect non-zero corrections at higher order.

As we eventually take the limit $\mathbf{b} \rightarrow 1$, we rewrite $\mathbf{b} = \exp(\delta\ell) \approx 1 + \delta\ell$ and will later take the limit $\delta\ell \rightarrow 0$. With $N \rightarrow 0$, we get the one-loop correlation to D , β , and Ω ($g_2 = \beta + i\Omega$) for model A:

$$g_0^< = g_0 \quad (A17a)$$

$$\beta^< = \beta - \beta \frac{g_0^2 M(1) S_d}{(\beta^2 + \Omega^2)(2\pi)^{d+1}} \left(\frac{1}{k^2} + \frac{4}{d} - 1 \right) \delta\ell \quad (A17b)$$

$$\Omega^< = \Omega + \Omega \frac{g_0^2 M(1) S_d}{(\beta^2 + \Omega^2)(2\pi)^{d+1}} \left(\frac{1}{k^2} + \frac{4}{d} - 1 \right) \delta\ell \quad (A17c)$$

$$D^< = D + D \frac{g_0^2 M(1) S_d}{(\beta^2 + \Omega^2)(2\pi)^{d+1}} \delta\ell \quad (A17d)$$

After rescaling the new value of the coupling constant for Model A become

$$g_0' = g_0(1 + \delta\ell)^{z-\gamma} \quad (A18a)$$

$$\beta' = \beta(1 + \delta\ell)^{z-2} \left(1 - \frac{g_0^2 Q_d}{\beta^2 + \Omega^2} \left(\frac{1}{k^2} + \frac{4}{d} - 1 \right) \right) \quad (A18b)$$

$$\Omega' = \Omega(1 + \delta\ell)^{z-2} \left(1 + \frac{g_0^2 Q_d}{\beta^2 + \Omega^2} \left(\frac{1}{k^2} + \frac{4}{d} - 1 \right) \right) \quad (A18c)$$

$$D' = D(1 + \delta\ell)^{(z-d-2\alpha)} \left(1 + \frac{g_0^2 Q_d}{\beta^2 + \Omega^2} \delta\ell \right) \quad (A18d)$$

where $Q_d = \frac{M(1)S_d}{(2\pi)^{d+1}}$ and it gives the RG flow equations for Model A:

$$\frac{dg_0}{d\ell} = g_0(z - \gamma) \quad (A19a)$$

$$\frac{d\beta}{d\ell} = \beta \left(z - 2 - \frac{g_0^2 Q_d}{\beta^2 + \Omega^2} \left(\frac{1}{k^2} + \frac{4}{d} - 1 \right) \right) \quad (A19b)$$

$$\frac{d\Omega}{d\ell} = \Omega \left(z - 2 + \frac{g_0^2 Q_d}{\beta^2 + \Omega^2} \left(\frac{1}{k^2} + \frac{4}{d} - 1 \right) \right) \quad (A19c)$$

$$\frac{dD}{d\ell} = D \left(z - d - 2\alpha + \frac{g_0^2 Q_d}{\beta^2 + \Omega^2} \right) \quad (A19d)$$

1. Integrals appearing in the Feynman diagrams

The integrals appearing in the Feynman diagrams for model A are given here.

$$D^{\text{corr}} = -\frac{g_0^2}{2} \int M(\mathbf{p}) \delta(\sigma) \frac{D}{g_2^2(\mathbf{k}-\mathbf{p})^4 + (\omega-\sigma)^2} \frac{d^d \mathbf{p}}{(2\pi)^d} \frac{d\sigma}{(2\pi)} \quad (\text{A20a})$$

$$\stackrel{\omega \rightarrow 0}{=} \left(-\frac{g_0^2 D}{2g_2^2 (2\pi)^{d+1}} \right) \int_{\mathbf{p}}^> \frac{M(\mathbf{p})}{(\mathbf{k}-\mathbf{p})^4} d^d \mathbf{p} \quad (\text{A20b})$$

$$= \left(-\frac{g_0^2 D}{2g_2^2 (2\pi)^{d+1}} \right) \int_{\Lambda(1-\delta\ell)}^{\Lambda} d\mathbf{p} \int_0^\pi d\theta \frac{\mathbf{p}M(\mathbf{p})}{(\mathbf{p}^2 + k^2 - 2k\mathbf{p} \cos \theta)^2} \mathbf{p}^{d-1} (\sin \theta)^{d-2} S_{d-1} \quad (\text{A20c})$$

$$\stackrel{\mathbf{p}=\Lambda}{\approx} \left(-\frac{g_0^2 D}{2g_2^2 (2\pi)^{d+1}} \right) \Lambda^d \delta\ell M(\Lambda) S_{d-1} \int_0^\pi d\theta \frac{(\sin \theta)^{d-2}}{(\Lambda^2 + k^2 - 2k\Lambda \cos \theta)^2} \quad (\text{A20d})$$

$$\stackrel{\Lambda=1}{=} \left(-\frac{g_0^2 D}{2g_2^2 (2\pi)^{d+1}} \right) \delta\ell M(1) S_{d-1} \int_0^\pi d\theta \frac{(\sin \theta)^{d-2}}{(1 + k^2 - 2k \cos \theta)^2} \quad (\text{A20e})$$

$$= \left(-\frac{g_0^2 D}{2g_2^2 (2\pi)^{d+1}} \right) \delta\ell M(1) S_{d-1} \int_0^\pi d\theta (\sin \theta)^{d-2} (1 - 2k^2 + 12k^2 \cos^2 \theta + \text{h.o.t.}) \quad (\text{A20f})$$

$$\approx \left(-\frac{g_0^2 D M(1)}{2g_2^2 (2\pi)^{d+1}} \right) \delta\ell S_{d-1} \left(\frac{S_d}{S_{d-1}} - 2k^2 \frac{S_d}{S_{d-1}} + 12k^2 \frac{1}{d} \frac{S_d}{S_{d-1}} \right) \quad (\text{A20g})$$

$$= \left(-\frac{1}{\beta^2 + \Omega^2} \frac{g_0^2 D M(1)}{4\pi} \frac{S_d}{(2\pi)^d} \right) \delta\ell \left(1 + k^2 \left(\frac{12}{d} - 2 \right) \right) \quad (\text{A20h})$$

$$= \left(-\frac{1}{\beta^2 + \Omega^2} \frac{g_0^2 D M(1)}{4\pi} \frac{S_d}{(2\pi)^d} \right) \delta\ell \quad (\text{A20i})$$

$$g_2^{\text{corr1}} = -\frac{g_0^2}{2} \int M(\mathbf{p}) \delta(\sigma) \frac{i}{g_2(\mathbf{k}-\mathbf{p})^2 - i(\omega-\sigma)} \frac{d^d \mathbf{p}}{(2\pi)^d} \frac{d\sigma}{(2\pi)} \quad (\text{A21a})$$

$$\stackrel{\omega \rightarrow 0}{=} -\frac{ig_0^2}{2g_2(2\pi)^{d+1}} \int_{\mathbf{p}}^> \frac{M(\mathbf{p})}{(\mathbf{k}-\mathbf{p})^2} d^d \mathbf{p} \quad (\text{A21b})$$

$$= -\frac{ig_0^2}{2g_2(2\pi)^{d+1}} \int_{\Lambda/b}^{\Lambda} d\mathbf{p} \int_0^\pi d\theta \frac{M(\mathbf{p})}{\mathbf{p}^2 + k^2 - 2k\mathbf{p} \cos \theta} \mathbf{p}^{d-1} (\sin \theta)^{d-2} S_{d-1} \quad (\text{A21c})$$

$$\stackrel{\mathbf{p}=\Lambda}{\approx} -\frac{ig_0^2}{2g_2(2\pi)^{d+1}} \Lambda^d \delta\ell M(\Lambda) S_{d-1} \int_0^\pi d\theta \frac{(\sin \theta)^{d-2}}{\Lambda^2 + k^2 - 2k\Lambda \cos \theta} \quad (\text{A21d})$$

$$\stackrel{\Lambda=1}{=} -\frac{ig_0^2}{2g_2(2\pi)^{d+1}} \delta\ell M(1) S_{d-1} \int_0^\pi d\theta \frac{(\sin \theta)^{d-2}}{1 + k^2 - 2k \cos \theta} \quad (\text{A21e})$$

$$= -\frac{ig_0^2}{2g_2(2\pi)^{d+1}} \delta\ell M(1) \int_0^\pi d\theta (\sin \theta)^{d-2} (1 - k^2 + 2k \cos \theta + 4k^2 \cos^2 \theta + \text{h.o.t.}) \quad (\text{A21f})$$

$$\approx -\frac{ig_0^2 M(1)}{2g_2(2\pi)^{d+1}} \delta\ell S_{d-1} \left(\frac{S_d}{S_{d-1}} - k^2 \frac{S_d}{S_{d-1}} + 0 + 4k^2 \frac{1}{d} \frac{S_d}{S_{d-1}} \right) \quad (\text{A21g})$$

$$= -\frac{ig_0^2 M(1)}{4\pi g_2} \frac{S_d}{(2\pi)^d} \delta\ell \left[1 + k^2 \left(\frac{4}{d} - 1 \right) \right] \quad (\text{A21h})$$

$$= \left(-\frac{\beta - i\Omega}{\beta^2 + \Omega^2} \frac{ig_0^2 M(1)}{4\pi} \frac{S_d}{(2\pi)^d} \right) \delta\ell \left[1 + k^2 \left(\frac{4}{d} - 1 \right) \right] \quad (\text{A21i})$$

$$g_2^{\text{corr}2} = -\frac{g_0^2}{2} \int \mathcal{M}(0) \frac{i}{g_2 p^2 - i\sigma} \frac{d^d \mathbf{p}}{(2\pi)^d} \frac{d\sigma}{(2\pi)} \quad (\text{A22a})$$

$$= -\frac{g_0^2 \mathcal{M}(0)}{2(2\pi)^{d+1}} \int_{\mathbf{p}} \int_{-\infty}^{\infty} d\sigma \frac{i}{g_2 p^2 - i\sigma} \quad (\text{A22b})$$

$$= -\frac{g_0^2 \mathcal{M}(0)}{2(2\pi)^{d+1}} \int_{\mathbf{p}} \int_{-\infty}^{\infty} d\sigma \frac{i}{(i\Omega + \beta)p^2 - i\sigma} \quad (\text{A22c})$$

$$= -\frac{g_0^2 \mathcal{M}(0)}{2(2\pi)^{d+1}} \int_{\mathbf{p}} 2\pi i \quad (\text{A22d})$$

$$= -\frac{i g_0^2 \mathcal{M}(0)}{2(2\pi)^d} \int_{\Lambda/b}^{\Lambda} p^{d-1} S_d dp \quad (\text{A22e})$$

$$\stackrel{p=\Lambda}{\approx} -\frac{i g_0^2 \mathcal{M}(0)}{2} \frac{S_d}{(2\pi)^d} \Lambda^d \delta\ell \quad (\text{A22f})$$

$$\stackrel{\Lambda=1}{=} -\frac{i g_0^2 \mathcal{M}(0) S_d}{2(2\pi)^d} \delta\ell \quad (\text{A22g})$$

$$g_0^{\text{corr}} = \frac{g_0^4}{4} \int \frac{i}{g_2 p^2 - i\sigma} \frac{i}{g_2 (\mathbf{p} - \mathbf{k})^2 - i(\sigma - \omega)} \frac{d^d \mathbf{p}}{(2\pi)^d} \frac{d\sigma}{(2\pi)} \quad (\text{A23a})$$

$$\stackrel{\omega \rightarrow 0}{=} \frac{g_0^4}{4} \int \frac{i}{g_2 p^2 - i\sigma} \frac{i}{g_2 (\mathbf{p} - \mathbf{k})^2 - i\sigma} \frac{d^d \mathbf{p}}{(2\pi)^d} \frac{d\sigma}{(2\pi)} \quad (\text{A23b})$$

$$= \frac{g_0^4}{4(2\pi)^{d+1}} \int_{\mathbf{p}} d^d \mathbf{p} \int_{-\infty}^{\infty} d\sigma \frac{i}{g_2 p^2 - i\sigma} \frac{i}{g_2 (\mathbf{p} - \mathbf{k})^2 - i\sigma} \quad (\text{A23c})$$

$$= 0 \quad (\text{A23d})$$

Appendix B: Replica Renormalization group analysis for Model B

The model B is given by

$$\partial_t \phi = (-g_1 \mathbf{m} \cdot \nabla + g_2 \nabla^2) \phi + I. \quad (\text{B1a})$$

$$\text{where } \langle m_i(\mathbf{x}) m_j(\mathbf{y}) \rangle \equiv M_{ij} = \delta_{ij} M(r), r = |\mathbf{x} - \mathbf{y}|, \quad (\text{B1b})$$

$$M(r) \sim r^{-\gamma} \quad (\text{B1c})$$

$$\text{and } \langle I(\mathbf{x}, t) I(\mathbf{y}, s) \rangle = D \delta^d(r) \delta(t - s) \equiv \tilde{D}. \quad (\text{B1d})$$

The Renormalization group calculation for model B is quite similar to that for model A and the only difference happens only for S_B^I :

$$S_B^I = g_1^2 \frac{1}{2} \sum_{\alpha, \beta}^N \mathbf{k}_2 \mathbf{k}_4 \Phi_\alpha(\mathbf{k}_1) \bullet \Phi_\alpha(\mathbf{k}_2) \bullet M(\mathbf{p}) \bullet \Phi_\beta(\mathbf{k}_3) \bullet \Phi_\beta(\mathbf{k}_4) \\ \times \delta(\mathbf{k}_1 + \mathbf{k}_2 - \mathbf{p}) \delta(\mathbf{k}_3 + \mathbf{k}_4 + \mathbf{p}) \quad (\text{B2a})$$

$$:= \quad (\text{B2b})$$

where the intersecting line on a straight line ($\phi(\mathbf{k}_2)$ or

$\phi(\mathbf{k}_4)$) represent \mathbf{k}_2 or \mathbf{k}_4 . As shown in Fig. 3, the corrections to g_2 , D , and g_1 are

$$g_2^{\text{corr}1} = \left(\frac{\beta - i\Omega}{\beta^2 + \Omega^2} \frac{i g_1^2 M(1) S_d}{2(2\pi)^{d+1}} \right) \delta\ell \left(1 - \frac{2}{d}\right) \mathbf{k}^2 \quad (\text{B3a})$$

$$g_2^{\text{corr}2} = 0 \quad (\text{B3b})$$

$$D^{\text{corr}} = -\frac{1}{\beta^2 + \Omega^2} \frac{g_1^2 D M(1)}{4\pi} \frac{S_d}{(2\pi)^d} \delta\ell \quad (\text{B3c})$$

$$g_1^{\text{corr}} = 0 \quad (\text{B3d})$$

The detail of the integrals are given in section B1. After rescaling in a manner same as model A we obtain the RG

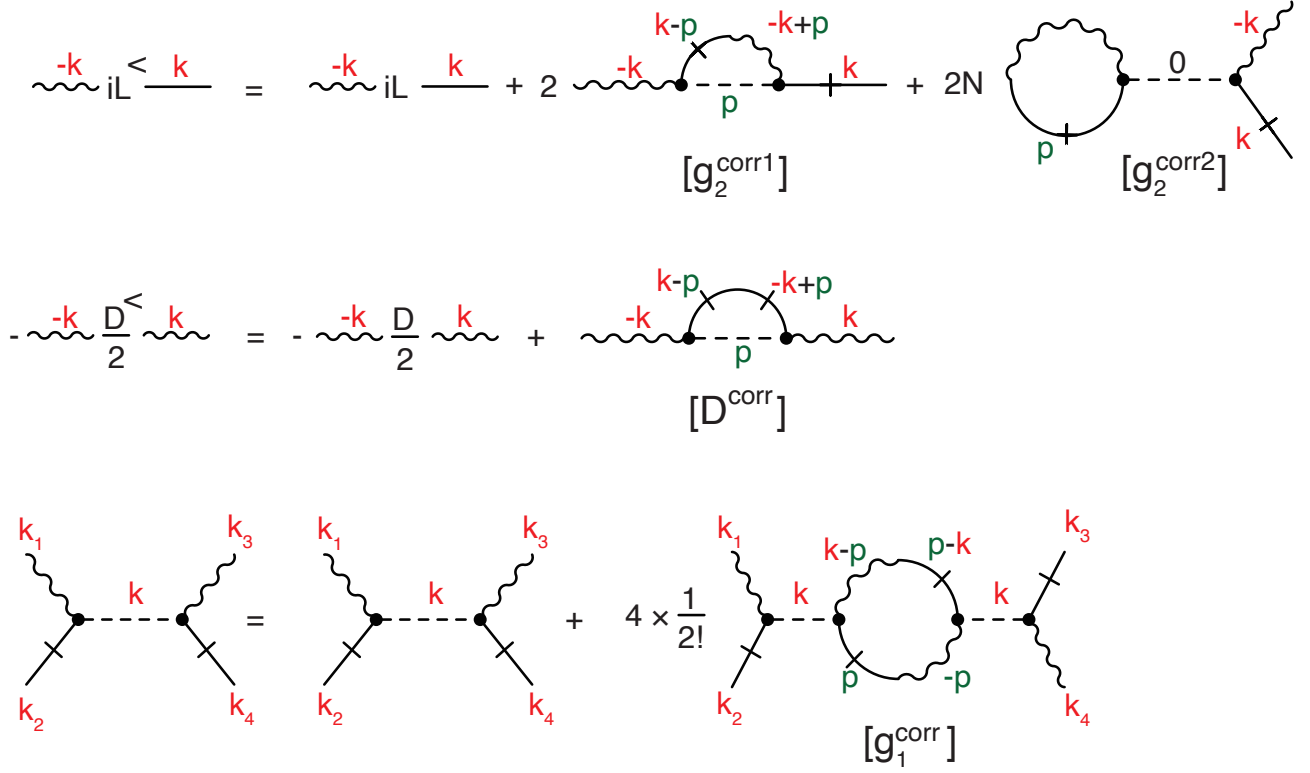


FIG. 3. The Feynman diagrams to calculate correction to g_0 , g_2 and D in model B up to one loop order. The short straight lines and short wavy lines denote ϕ and Φ respectively. The long straight line denotes the free correlation function and the long line with one wavy end and other straight end denotes the free Green's function. Additionally, an intersecting line on a straight line ($\phi(\mathbf{k}_2)$ or $\phi(\mathbf{k}_4)$) represents \mathbf{k}_2 or \mathbf{k}_4 .

flow equations for Model B:

$$\frac{dg_1}{dl} = g_1(z - \gamma - 1) \quad (\text{B4a})$$

$$\frac{d\beta}{dl} = \beta \left(z - 2 + \frac{g_1^2 Q_d}{\beta^2 + \Omega^2} \left(1 - \frac{2}{d} \right) \right) \quad (\text{B4b})$$

$$\frac{d\Omega}{dl} = \Omega \left(z - 2 - \frac{g_1^2 Q_d}{\beta^2 + \Omega^2} \left(1 - \frac{2}{d} \right) \right) \quad (\text{B4c})$$

$$\frac{dD}{dl} = D \left(z - d - 2\alpha + \frac{g_1^2 Q_d}{\beta^2 + \Omega^2} \right) \quad (\text{B4d})$$

where $Q_d = \frac{M(1)S_d}{(2\pi)^{d+1}}$.

1. Integrals appearing in the Feynman diagrams

The integrals appearing in the Feynman diagrams for model B are given here.

$$D^{\text{corr}} = \left(\frac{g_1^2}{2}\right) \int M(\mathbf{p}) \delta(\sigma) \frac{D}{g_2^2(\mathbf{k}-\mathbf{p})^4 + (\omega-\sigma)^2} - (\mathbf{k}-\mathbf{p})^2 \frac{d^d \mathbf{p}}{(2\pi)^d} \frac{d\sigma}{(2\pi)} \quad (\text{B5a})$$

$$\stackrel{\omega \rightarrow 0}{=} \left(-\frac{g_1^2 D}{2g_2^2(2\pi)^{d+1}}\right) \int_{\mathbf{p}}^> \frac{M(\mathbf{p})}{(\mathbf{k}-\mathbf{p})^2} d^d \mathbf{p} \quad (\text{B5b})$$

$$= \left(-\frac{g_1^2 D}{2g_2^2(2\pi)^{d+1}}\right) \int_{\Lambda(1-\delta\ell)}^{\Lambda} d\mathbf{p} \int_0^{\pi} d\theta \frac{\mathbf{p}M(\mathbf{p})}{p^2 + k^2 - 2kp \cos \theta} p^{d-1} (\sin \theta)^{d-2} S_{d-1} \quad (\text{B5c})$$

$$\stackrel{\mathbf{p}=\Lambda}{\approx} \left(-\frac{g_1^2 D}{2g_2^2(2\pi)^{d+1}}\right) \Lambda^d \delta\ell M(\Lambda) S_{d-1} \int_0^{\pi} d\theta \frac{(\sin \theta)^{d-2}}{\Lambda^2 + k^2 - 2k\Lambda \cos \theta} \quad (\text{B5d})$$

$$\stackrel{\Lambda=1}{=} \left(-\frac{g_1^2 D}{2g_2^2(2\pi)^{d+1}}\right) \delta\ell M(1) S_{d-1} \int_0^{\pi} d\theta \frac{(\sin \theta)^{d-2}}{1 + k^2 - 2k \cos \theta} \quad (\text{B5e})$$

$$= \left(-\frac{g_1^2 D}{2g_2^2(2\pi)^{d+1}}\right) \delta\ell M(1) S_{d-1} \int_0^{\pi} d\theta (\sin \theta)^{d-2} (1 - k^2 + 4k^2 \cos^2 \theta + \text{h.o.t.}) \quad (\text{B5f})$$

$$\approx \left(-\frac{g_1^2 DM(1)}{2g_2^2(2\pi)^{d+1}}\right) \delta\ell S_{d-1} \left(\frac{S_d}{S_{d-1}} - k^2 \frac{S_d}{S_{d-1}} + 4k^2 \frac{1}{d} \frac{S_d}{S_{d-1}}\right) \quad (\text{B5g})$$

$$= \left(-\frac{1}{\beta^2 + \Omega^2} \frac{g_1^2 DM(1)}{4\pi} \frac{S_d}{(2\pi)^d}\right) \delta\ell \left(1 + k^2 \left(\frac{4}{d} - 1\right)\right) \quad (\text{B5h})$$

$$\approx \left(-\frac{1}{\beta^2 + \Omega^2} \frac{g_1^2 DM(1)}{4\pi} \frac{S_d}{(2\pi)^d}\right) \delta\ell \quad (\text{B5i})$$

$$g_2^{\text{corr1}} = \frac{g_1^2}{2} \int M(\mathbf{p}) \delta(\sigma) \frac{i(\mathbf{k}-\mathbf{p}) \cdot \mathbf{k}}{g_2(\mathbf{k}-\mathbf{p})^2 - i(\omega-\sigma)} \frac{d^d \mathbf{p}}{(2\pi)^d} \frac{d\sigma}{(2\pi)} \quad (\text{B6a})$$

$$\stackrel{\omega \rightarrow 0}{=} \frac{ig_1^2}{2g_2(2\pi)^{d+1}} \int_{\mathbf{p}}^> \frac{M(\mathbf{p})(\mathbf{k}-\mathbf{p}) \cdot \mathbf{k}}{(\mathbf{k}-\mathbf{p})^2} d^d \mathbf{p} \quad (\text{B6b})$$

$$= \frac{ig_1^2}{2g_2(2\pi)^{d+1}} \int_{\Lambda/b}^{\Lambda} d\mathbf{p} \int_0^{\pi} d\theta \frac{M(\mathbf{p})(k^2 - kp \cos \theta)}{p^2 + k^2 - 2kp \cos \theta} p^{d-1} (\sin \theta)^{d-2} S_{d-1} \quad (\text{B6c})$$

$$\stackrel{\mathbf{p}=\Lambda}{\approx} \frac{ig_1^2}{2g_2(2\pi)^{d+1}} \Lambda^d \delta\ell M(\Lambda) S_{d-1} \int_0^{\pi} d\theta \frac{(\sin \theta)^{d-2} (k^2 - k\Lambda \cos \theta)}{\Lambda^2 + k^2 - 2k\Lambda \cos \theta} \quad (\text{B6d})$$

$$\stackrel{\Lambda=1}{=} \frac{ig_1^2}{2g_2(2\pi)^{d+1}} \delta\ell M(1) S_{d-1} \int_0^{\pi} d\theta \frac{(\sin \theta)^{d-2} (k^2 - k \cos \theta)}{1 + k^2 - 2k \cos \theta} \quad (\text{B6e})$$

$$= \frac{ig_1^2}{2g_2(2\pi)^{d+1}} \delta\ell M(1) \int_0^{\pi} d\theta (\sin \theta)^{d-2} (k^2 - 2k^2 \cos^2 \theta + \text{h.o.t.}) \quad (\text{B6f})$$

$$\approx \frac{ig_1^2 M(1)}{2g_2(2\pi)^{d+1}} \delta\ell S_{d-1} \left(k^2 \frac{S_d}{S_{d-1}} - 2k^2 \frac{1}{d} \frac{S_d}{S_{d-1}}\right) \quad (\text{B6g})$$

$$= \frac{ig_1^2 M(1)}{4\pi g_2} \frac{S_d}{(2\pi)^d} \delta\ell \left(1 - \frac{2}{d}\right) k^2 \quad (\text{B6h})$$

$$= \left(\frac{\beta - i\Omega}{\beta^2 + \Omega^2} \frac{ig_1^2 M(1)}{4\pi} \frac{S_d}{(2\pi)^d}\right) \delta\ell \left(1 - \frac{2}{d}\right) k^2 \quad (\text{B6i})$$

$$g_2^{\text{corr}2} = \frac{g_1^2}{2} \int M(0) \frac{i\mathbf{p} \cdot \mathbf{k}}{g_2 p^2 - i\sigma} \frac{d^d \mathbf{p}}{(2\pi)^d} \frac{d\sigma}{(2\pi)} \quad (\text{B7a})$$

$$= \frac{g_1^2 M(0)}{2(2\pi)^{d+1}} \int_{\mathbf{p}}^> d^d \mathbf{p} \int_{-\infty}^{\infty} d\sigma \frac{i\mathbf{p} \cdot \mathbf{k}}{g_2 p^2 - i\sigma} \quad (\text{B7b})$$

$$= \frac{g_1^2 M(0)}{2(2\pi)^{d+1}} \int_{\mathbf{p}}^> d^d \mathbf{p} \int_{-\infty}^{\infty} d\sigma \frac{i\mathbf{p} \cdot \mathbf{k}}{(i\Omega + \beta)p^2 - i\sigma} \quad (\text{B7c})$$

$$= \frac{g_1^2 M(0)}{2(2\pi)^{d+1}} \int_{\mathbf{p}}^> \mathbf{p} \cdot \mathbf{k} d^d \mathbf{p} 2\pi i \quad (\text{B7d})$$

$$= 0 \quad (\text{B7e})$$

$$g_0^{\text{corr}} = \frac{g_1^4}{4} \int \frac{i}{g_2 p^2 - i\sigma} \frac{i}{g_2 (\mathbf{p} - \mathbf{k})^2 - i(\sigma - \omega)} \mathbf{p} \cdot (\mathbf{p} - \mathbf{k}) \frac{d^d \mathbf{p}}{(2\pi)^d} \frac{d\sigma}{(2\pi)} \quad (\text{B8a})$$

$$\stackrel{\omega \rightarrow 0}{=} \frac{g_1^4}{4} \int \frac{i}{g_2 p^2 - i\sigma} \frac{i}{g_2 (\mathbf{p} - \mathbf{k})^2 - i\sigma} \mathbf{p} \cdot (\mathbf{p} - \mathbf{k}) \frac{d^d \mathbf{p}}{(2\pi)^d} \frac{d\sigma}{(2\pi)} \quad (\text{B8b})$$

$$= \frac{g_1^4}{4(2\pi)^{d+1}} \int_{\mathbf{p}}^> d^d \mathbf{p} \int_{-\infty}^{\infty} d\sigma \frac{i}{g_2 p^2 - i\sigma} \frac{i}{g_2 (\mathbf{p} - \mathbf{k})^2 - i\sigma} \mathbf{p} \cdot (\mathbf{p} - \mathbf{k}) \quad (\text{B8c})$$

$$= 0 \quad (\text{B8d})$$

Appendix C: Useful identities in d dimensions

The surface area and volume of the unit sphere in d dimensions are, respectively,

$$S_d = \frac{2\pi^{d/2}}{\Gamma(d/2)} \quad (\text{C1a})$$

$$V_d = \frac{\pi^{d/2}}{\Gamma(d/2 + 1)} \quad (\text{C1b})$$

where Γ is the Gamma function. Volume element in spherical coordinate in d dimensions

$$d^d \mathbf{V} = r^{d-1} \sin^{d-2}(\theta_1) \sin^{d-3}(\theta_2) \dots \sin^{d-2}(\theta_{d-2}) dr d\theta_1 \dots d\theta_{d-1} \quad (\text{C2})$$

The integration of a function that depends only on the magnitude of wavevector \mathbf{k} in d dimensions

$$\int f(k) d^d \mathbf{k} = S_d \int_0^{\infty} f(k) k^{d-1} dk \quad (\text{C3})$$

Few other useful integrals [see, e.g., 37, Appendix B]

$$\int_0^{\pi} \sin^{d-2} \theta d\theta = \frac{S_d}{S_{d-1}} \quad (\text{C4a})$$

$$\int_0^{\pi} \sin^{d-2} \theta \cos \theta = 0 \quad (\text{C4b})$$

$$\int_0^{\pi} \sin^{d-2} \theta \cos^2 \theta = \frac{1}{d} \frac{S_d}{S_{d-1}} \quad (\text{C4c})$$